



Nanoparticles of niobium oxyhydroxide incorporated in different polymers for photocatalytic degradation of dye

Ana Pacheli Heitmann¹ · Italo Coura Rocha² · Iaci Miranda Pereira³ · Luiz Carlos Alves Oliveira¹ · Patrícia Santiago de Oliveira Patrício²

Received: 5 October 2018 / Accepted: 29 May 2019 / Published online: 6 June 2019
© The Polymer Society, Taipei 2019

Abstract

In this work, it has been reported the preparation of catalytic systems based on chemically modified niobium oxides and different polymer matrices, polypropylene (PP), poly(3-hydroxybutyrate) (PHB) and polyurethane (WPU). The efficiency of systems as photocatalysis was investigated. Materials prepared from various polymer matrices showed distinct photocatalytic activities. The systems based on PHB matrix and niobium oxyhydroxide presenting the best performance among the studied systems, ~ 90% dye removal at 60 min. The results of systems characterization by Scanning Electron Microscopy (SEM), Infrared Spectroscopy (FTIR) and Differential Scanning Calorimetry (DSC) analysis technical have showed that nanoparticles size, their dispersion in the polymeric matrix and interaction polymer-inorganic particles are responsible by changing photocatalysis process. However, for the PHB, structure parameters of matrix are important. The synchrotron radiation was used to investigate the macromolecular structure of the pure polymers and after the incorporation of niobium nanoparticles.

Keywords Polymer composites · Niobium oxyhydroxide · Photocatalysis

Introduction

Photocatalytic degradation has attracted great interest as a technique for the removal of organic and inorganic contaminants in residual water generated by oil refinery, textile and tanneries [1]. This process promotes an almost complete degradation of difficult oxidation organic pollutants to simple compounds such as CO₂ and H₂O besides using sunlight as a source of clean energy [2]. However, the implantation of photocatalytic systems in industrial scale has technological

limitations, as the difficulty of building large light collectors to treat great volumes of effluents and especially the separation of the semiconductor from the aqueous medium [3].

Semiconductors, mainly TiO₂, are widely studied in photocatalytic reactions [4] because its chemical stability, low toxicity and commercial availability. Nevertheless, the effect of the high recombination rate of the electron-hole pairs on TiO₂ reduces photocatalytic efficiency and limits its industrial application [5]. Another alternative is niobium-based catalysts that have been studied in the photodegradation of organic pollutants in aqueous medium and acting with similar efficiency under UV radiation in comparison to TiO₂ [6]. Brazil has the largest reserves of niobium in the world. The niobium oxide has specific properties that highlight it as a catalyst, especially in the presence of Lewis and Brønsted acid sites, high chemical and thermal stabilities [7]. Niobium catalysts, mainly the nanometric sized oxides have been used as active phases or as support of other metals in various reactions including photocatalysis [8].

One of the approaches to solving the difficulty of recovering the catalyst from the aqueous medium is its combination with other materials, such as ceramics, glass, metals and polymers. According to Singh et al. [9], the polymers represent a

✉ Ana Pacheli Heitmann
anapacheli@gmail.com

¹ Department of Chemistry, Universidade Federal de Minas Gerais, Av. Antônio Carlos 6627, Campus Pampulha, 31270-901, BH-, Belo Horizonte, MG, Brazil

² Department of Chemistry, Centro Federal de Educação Tecnológica de Minas Gerais, CEFET-MG, Av. Amazonas 5253, 30421-169, BH-, Belo Horizonte, MG, Brazil

³ Centro Tecnológico do Exército, Av. Américas, 28705, Guaratiba, Rio de Janeiro, RJ 23020-470, Brazil

viable alternative to be used as a support for inorganic photocatalysts. Their important properties are: (i) chemically inert to the medium, (ii) hydrophobicity allows them to retain the pollutants on their surface, leading to an increased efficiency both in the adsorption and perhaps in the oxidation; (iii) are accessible and can be found with abundance; (iv) low density (float in the aqueous medium), being easily removed. In addition, the immobilization of the catalyst may lead to the optimization of light absorption.

Nowadays, highlighted studies of inorganic catalytic-polymer systems applied to photocatalysis reported in the literature: polystyrene (PS)/TiO₂ films [10], high density polyethylene (HDPE) discs with TiO₂ coated surface [11] both used for degradation of the methylene blue dye in the presence of UV radiation. The polyethylene terephthalate (PET/TiO₂) system used for the oxidation of As (III) to As (V) and the removal of As (V) from the aqueous medium in the presence of iron (II) oxyhydroxide and sunlight [12]. The polyaniline composite (PANI/TiO₂) used for the degradation of methylene blue in the presence of visible radiation [13]. However, sophisticated and expensive methods for impregnation of the catalysts in the matrix, such as sol-gel process, in situ chemical polymerization, coating and spray technique cause the development of these materials on a large scale costly. Additionally, all polymers investigated are of synthetic origin making the degradation process difficult when released into the environment. In a pioneering work, our research group investigated the incorporation of different nanoparticles of niobium oxyhydroxide in the poly (3-hydroxybutyrate) PHB matrix, biodegradable polymer, changing the oxide content [14] and the morphology of the polymer matrix [15]. The photocatalytic degradation efficiency of the methylene blue dye using UV radiation was investigated. Photocatalysis experiments were carried out under continuous flow and exposed to UV radiation. The degradation of ~ 100% of the dye was observed with the formation of intermediary species indicating the advanced stage of oxidation of the organic molecule [14].

The main goal of this work is to investigate the performance of different polymeric matrixes acting as support to niobium oxyhydroxide based catalyst. The polymers become interesting supports for inorganic semiconductors only if the catalytic activity is preserved in the polymer-catalyst system. In this context, chemical interactions between polymer and catalyst can become relevant. Inorganic oxides have chemical groups in their structure with high polarity contrasting with most polymers. Here, polymeric matrixes have different chemical structures, polypropylene (PP), poly(3-hydroxybutyrate) (PHB) and polyurethane (WPU) were investigated. The PP has only C-H bonds in its structure, the PHB has in addition carbonyl groups and the urethane group is composed of C=O, C-O-C and N-H bonds. These groups are responsible for conferring different polarities to the polymers, increasing in the following order PP < PHB < WPU. The

polymer-inorganic catalyst systems have been developed and characterized by scanning electron microscopy (SEM), infrared spectroscopy (FTIR) and differential scanning calorimetry (DSC) analyze techniques. The crystallinity reduction of polymers from the disordered growth of their crystals may influence in the photocatalytic activity of the polymers. Although crystallinity is a complex factor, a low crystallinity usually caused by the presence of impurities, micro-holes and vacancies, has been reported to increase the photocatalytic activity. Active centers are provided for oxidation/reduction reactions through the production of defects in the polymer structure [16]. Then, the polymer crystalline structure was studied using Small Angle X-Ray Scattering (SAXS). The photocatalytic efficiency of polymer-catalytic systems was evaluated from the kinetic curves of the removal of methylene blue (model molecule) from aqueous medium with UV light.

Experimental

Catalytic syntheses: niobium oxyhydroxide (NbO₂(OH))

For synthesis of the niobium oxyhydroxide (NbO₂(OH)), 46.2 mmol of the ammonium oxalate salt of niobium (NH₄[NbO(C₂O₄)₂(H₂O)](H₂O)_n) was dissolved in distilled water under heating at 90 °C. After the complete dissolution of the salt, NH₄OH was slowly added to the solution until pH 7 was reached, for precipitation of the niobium oxyhydroxide. Thereafter, the suspension was kept under constant stirring for 12 h for aging. Finally, the resulting white solid was filtered, washed and oven dried for 12 h [17].

The obtained material was dispersed in distilled water and treated with 30% hydrogen peroxide. The resulting yellow solid was filtered, washed with distilled water and dried for 12 h. The catalytic activity of this material is addressed in the various oxidation reactions described by our research group [18]. Therefore, the characterization of this material has already been explored and shows that the yellow solid is a nanoparticulate material.

Composite preparation

The polymer/catalyst systems were prepared using three different polymer matrixes: (i) polypropylene (PP), (ii) poly (3-hydroxybutyrate) (PHB), (iii) polyurethane (PU). The methods of preparing the materials are dependent on the polymers used, as described below.

Film by casting

The films of PHB/NbO₂(OH) were obtained by the casting technique. For the preparation of films, the PHB powder

(BIOCYCLE®, Molecular weight = 600 Kg.mol⁻¹) was solubilized in chloroform and dimethylformamide at a ratio of 1:5, to which niobium oxyhydroxide content was of 2% wt. The solution was placed under constant agitation and heated at approximately 55 °C until complete dissolution over 4 h. The mixture was poured into glass Petri dishes, and the solvent was left to evaporate at room temperature for 72 h, after which the samples were put in the oven at 60 °C for 24 h. The nanocomposite PHB/NbO₂(OH) was obtained by similar method.

The WPU was synthesized by pre-polymer method as described in our previous work [19]. The reagents used in the first step were in the, diisocianato de isoforona (IPDI – Bayer), a mixture of 75 wt% polycarbonate (PC MM = 1000–2000 g.mol⁻¹) and 25 wt% of polypropyleneglycol (PPG MM = 1000–2000 g.mol⁻¹), dimethylolpropionic acid (DMPA) (Sigma Aldrich) and triethylamine (TEA) (Merck). After the obtention of pre-polymer it was dispersed in water and hydrazine (HI) was added. The dibutyltin dilaurate (DBTDL – Sigma Aldrich) was used as catalytic of polymerization.

For the obtention of nanocomposite WPU/NbO₂(OH), 2 wt% was introduced in the reaction flask after of HI addition. The waterborne polyurethane were filtered in the nylon screens to eliminate coarse particles.

Mechanical processing

The pure PP (Brasken 9.1 Kg. mol⁻¹) and the mixture of PP and NbO₂(OH) catalyst (2 wt%) were added to a Thermo Haake (Polydrive mixer) mixing chamber at a temperature of 180 °C for 5 min. After cooling, the obtained mixture was added to a knife mill (Mill KIE 600). Pressing was conducted in several steps at 180 °C for 3 min at 2 MPa, and the films were cooled at room temperature.

Catalytic tests

The catalytic tests were performed at 25 °C using 15 mL of methylene blue solution (20 mg.L⁻¹) as the model molecule. A 0.5 g aliquot of the polymer film was used, with stirring at 330 rpm using a magnetic stirrer for predetermined times of 10–120 min. A UV lamp was used (mercury vapor $\lambda = 254$ nm) with power of 15 W. The samples were positioned at 20 cm from the UV light. The oxidation efficiency was monitored with a UV-Vis spectrophotometer (Shimadzu UV-1601-PC) at wavelengths of 664 nm.

Characterization of materials

The morphology of the developed composites was characterized by a scanning electron microscope (SEM) (JEOL, model 840A) operating at 7 kV. The samples were introduced in the

liquid-nitrogen and the cryofracture surface was analyzed. The films were coated with a 5 nm carbon layer using a BAL-TEC 010 MC instrument after they were put into a microscope. EDS spectra were obtained from the images performed using backscattered electrons with voltage of 7 kV, spotsize 27, magnitude 400 in vacuum atmosphere.

Infrared spectroscopic (FTIR) data were obtained with a Shimadzu Prestige 21 spectrophotometer equipped with an attenuated total reflection accessory (ATR with Krs-5 crystal) in reflection mode. The spectra were collected in the range of 4000 to 400 cm⁻¹ with a scan number of 60 and resolution of 4 cm⁻¹.

The synchrotron small angle X-ray scattering experiments were performed on the beam line at the National Synchrotron Light Laboratory (LNLS, Campinas, Brazil). The monochromatized wavelength was 1.55 Å. The data were corrected for the parasitic scattering intensity produced by the collimating slits, the non-constant sensitivity of the position sensitive X-ray detector, the time varying intensity of the direct synchrotron beam, and the differences in specimen thickness. SAXS measurements were performed using the MAR-165 detector. During the measurements, two different sample-detector distances were used: Distance A, 2132 mm, and Distance B, 603 mm.

The DSC curves were obtained on a TA Instruments DSC2010 thermo analyzer. The samples were put into a hermetically sealed alumina pan. In the first run, the samples were heated in the temperature range from 30 to 185 °C, maintained at final temperature for 3 min, cooled to -30 °C and heated again to 190 °C at a rate of 10 °C min⁻¹ under a dynamic nitrogen atmosphere (50 mL min⁻¹). The DSC curves shown are for the second run of heating. The crystallinity index (X_c) of the polymers and the polymers/niobium oxyhydroxide composites was calculated from Eq. 1:

$$X_c = \frac{\Delta H_n \times 100}{\Delta H_{0xw}(\text{polymer})} \quad (1)$$

Where ΔH is the melting enthalpy of the sample (J.g⁻¹) as the heat of fusion for 100% crystalline polymers and w is the weight fraction of the polymer's samples [20]. Para o PHB o valor de ΔH foi 146 J.g⁻¹ e para o PP, 209 J.g⁻¹.

Results and discussion

Photocatalytic experiment

The kinetic curves obtained from the removal of methylene blue from aqueous medium in the presence of the catalytic systems and UV radiation are shown in the Fig. 1. The catalyst systems PHB/NbO₂(OH) and PP/NbO₂(OH) present similar removal of the dye by adsorption process, close to 20%, as

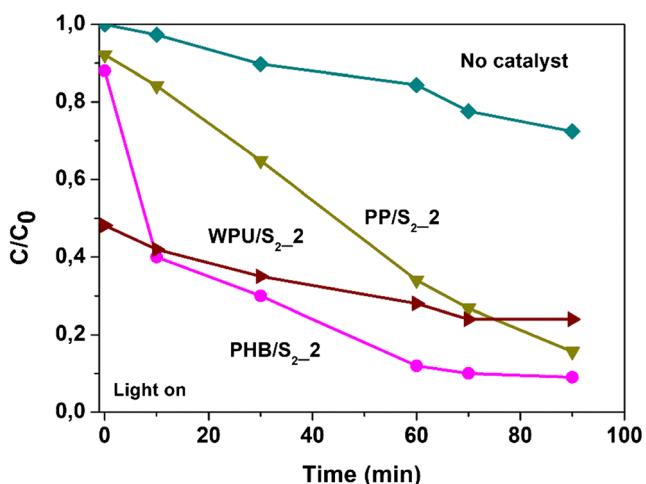


Fig. 1 Kinetic of methylene blue dye removal from aqueous medium with catalytic system and UV light ($S_2 = \text{NbO}_2(\text{OH})$)

WPU/ $\text{NbO}_2(\text{OH})$ removes $\sim 50\%$ of the dye. Another important process is the photolysis, which is represented for “no catalyst” curve in the Fig. 1 responsible for $\sim 30\%$ of dye photodegradation at 90 min.

After 90 min the removal of dye from aqueous medium was of $\sim 40\%$ with PP/ $\text{NbO}_2(\text{OH})$, $\sim 80\%$ with WPU/ $\text{NbO}_2(\text{OH})$ and $\sim 90\%$ with PHB/ $\text{NbO}_2(\text{OH})$. Some peculiarities are observed to the systems: (i) PHB/ $\text{NbO}_2(\text{OH})$ and WPU/ $\text{NbO}_2(\text{OH})$ achieved the maximum of dye removal at 60 min; (ii) to WPU/ $\text{NbO}_2(\text{OH})$, the adsorption process is more significantly than the photocatalysis in the dye removal (iii) when incorporated in the PHB the niobium nanoparticle maintained its ability to act as a catalyst; (iv) to PHB/ $\text{NbO}_2(\text{OH})$ the removal of dye is more pronounced in the initial 10 min of photocatalytic process; and (v) the removal of methylene blue by PP/ $\text{NbO}_2(\text{OH})$ is mainly due to photolysis process.

Despite the low efficiency of PP/ $\text{NbO}_2(\text{OH})$ as catalyst the removal of ethylene blue is still slightly higher than in the literature works [21] utilizing impregnated TiO_2 in the PP beads. Moreover, the method of preparation used here is easier than impregnation methods.

Characterization of the composites

SEM images and EDS spectra obtained from catalytic systems polymer/ $\text{NbO}_2(\text{OH})$ are shown in the Fig. 2. The fracture morphology of PP and PP/ $\text{NbO}_2(\text{OH})$ is typical of ductile polymers with rough surfaces. Pores were not observed in the magnification used [22]. In the PP/ $\text{NbO}_2(\text{OH})$ SEM image appears only one phase, probably the $\text{NbO}_2(\text{OH})$ nanoparticle size is too small to be seen with this magnification. However, the Nb peak in the EDS spectrum confirms the presence of $\text{NbO}_2(\text{OH})$ nanoparticle in the sample. The PP/ $\text{NbO}_2(\text{OH})$ has been prepared by mechanical processing, which both,

polymer and nanoparticle, were under high shear and temperature. It is believed that in these conditions the niobium oxyhydroxide agglomerates had their size reduced resulting in a good nanoparticle dispersion in the matrix.

SEM image of PHB reveals a brittle fracture morphology as expected for this polymer, fracture propagation in one direction. PHB/ $\text{NbO}_2(\text{OH})$ images shows two phases, one has a morphology similar to the matrix, and a second brighter phase with its size submicrometric. The second phase visualized in the SEM images of PHB/ $\text{NbO}_2(\text{OH})$ was attributed as $\text{NbO}_2(\text{OH})$ agglomerates, supported by the EDS spectrum obtained while focusing this region registering the Nb peak.

For the WPU, the fracture morphology presents a smooth and dense phase, similar to the ductile fracture, although the cracks were observed after the extensive plastic deformation. On the other hand, the WPU/ $\text{NbO}_2(\text{OH})$ presents more brittleness indicating that the $\text{NbO}_2(\text{OH})$ nanoparticle was able to influence the WPU fracture mode. Probably, the chemical interactions between polymer and nanoparticles may have led to such changes [23] and they contribute to that $\text{NbO}_2(\text{OH})$ not being visible in the SEM image. The WPU/ $\text{NbO}_2(\text{OH})$ EDS spectrum shows the presence of the niobium nanoparticles.

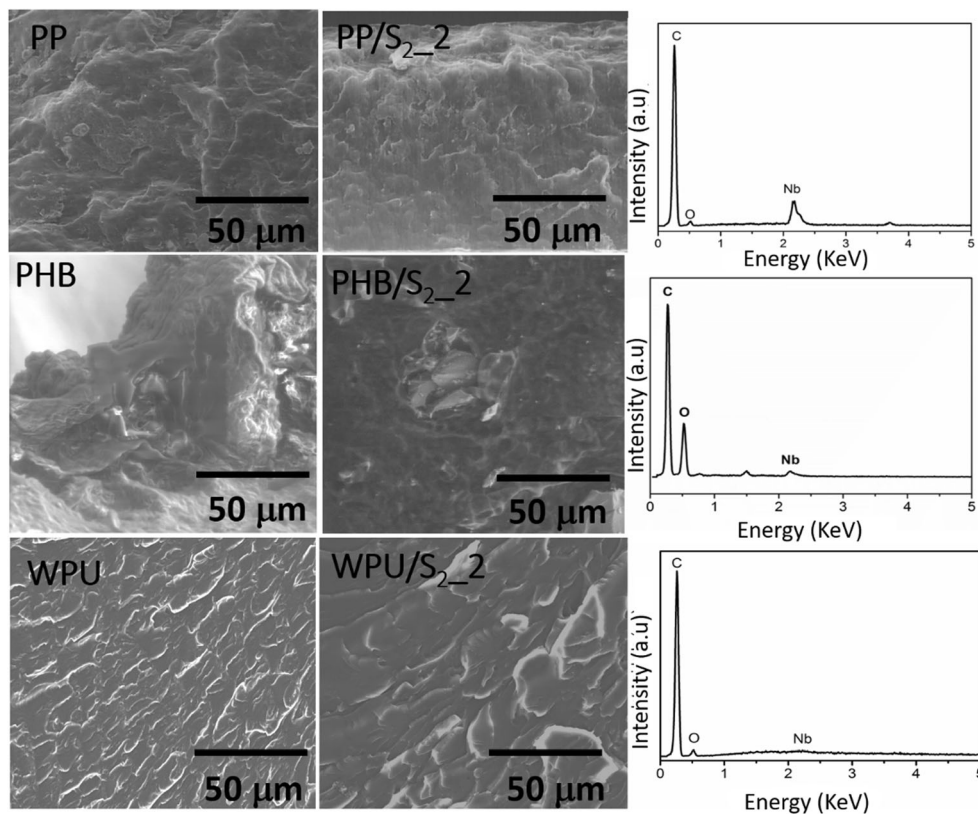
Comparing the SEM images of nanocomposites with the three polymeric matrixes it can be concluded that nanoparticle is better dispersed in WPU/ $\text{NbO}_2(\text{OH})$ and PP/ $\text{NbO}_2(\text{OH})$ systems. These results can be explained by two different ways: (i) chemical affinity (probably associated with a higher hydrophilicity) and (ii) the efficiency of the mixture method. Highlighting that the $\text{NbO}_2(\text{OH})$ was introduced during the WPU synthesis, promoting additionally a more favorable condition to the nanoparticle-polymer interaction.

The chemical interactions were investigated by FTIR, the spectra are shown in the Fig. 3.

FTIR spectra of PP and PP/ $\text{NbO}_2(\text{OH})$, Fig. 3a, shows the polymer bands in the range of ~ 3000 and 2800 cm^{-1} and ~ 1500 and 800 cm^{-1} , that are associated with the stretching vibrations and deformations of C-H bonds, respectively [24, 25]. The addition of catalyst nanoparticles did not promote significant change of PP spectrum because, mainly, of the poor chemical affinity between polymer nanoparticle. The PP structure is non-polar in contrast with the high $\text{NbO}_2(\text{OH})$ polarity.

In the PHB and PHB/ $\text{NbO}_2(\text{OH})$ spectra shown in the Fig. 3b, it can be observed characteristic bands of PHB spectrum. The bands at 1720 cm^{-1} and shoulder at 1745 cm^{-1} are associated to the stretching vibrations of C=O ester and those at 1272 and 980 cm^{-1} to the stretching vibrations C-O-C groups. The band at 1185 cm^{-1} resulting from the vibration of amorphous phases of groups of polymers in contrast with bands at 1228 , 1272 cm^{-1} relative to the crystalline phases. These bands are important in the identification of PHB structure by FTIR analyses [26]. However, the relative number of

Fig. 2 SEM images of cryofracture surface of pure polymers (left) and catalytic systems polymers/NbO₂(OH) (in the middle column), and EDS spectra obtained from regions of the image (right) (S₂ = NbO₂(OH))



interactions polymer-catalyst achieved is too small to promote higher changes in the spectrum due to content low in NbO₂(OH).

In the Fig. 3c are shown the WPU and WPU/NbO₂(OH) FTIR spectra. Two of the mains bands in the WPU study are referent to N-H group stretching and deformation vibration which appears respectively at 3310 and 1533 cm⁻¹ [27]. Over again the carbonyl band is important to this polymer, it is displayed at 1741 cm⁻¹ [28]. In order to investigate possible interactions between NbO₂(OH) and WPU in the region at 1800–1600 cm⁻¹ were done deconvolution and Gaussian adjustments, Fig. 2c.

Six bands were revealed in the carbonyl region of WPU and WPU/NbO₂(OH) spectra due to free and hydrogen bond

C=O, of urea at 1665 e 1642 cm⁻¹, and urethane at 1720 e 1702 cm⁻¹ groups, respectively [29]. However, the bands appear shifted to lower frequencies in the WPU/NbO₂(OH) spectrum indicating a formation of hydrogen interactions between WPU and NbO₂(OH). The rate of the areas (R) from a carbonyl band involved in hydrogen bond and free carbonyl band from urethane groups is known as a semi-quantitative parameter FTIR analysis to study of the new hydrogen bond formed. The R is 1.6 to WPU and 1.9 to WPU/NbO₂(OH). The higher is the R value of the finding, the lower is the content of free C=O. The increase of R suggests that the hydrogen bonds between catalyst –OH groups and C=O polyurethane. Other polyurethane groups as C-O-C or N-H could be involved in hydrogen bond with catalyst–OH but it would

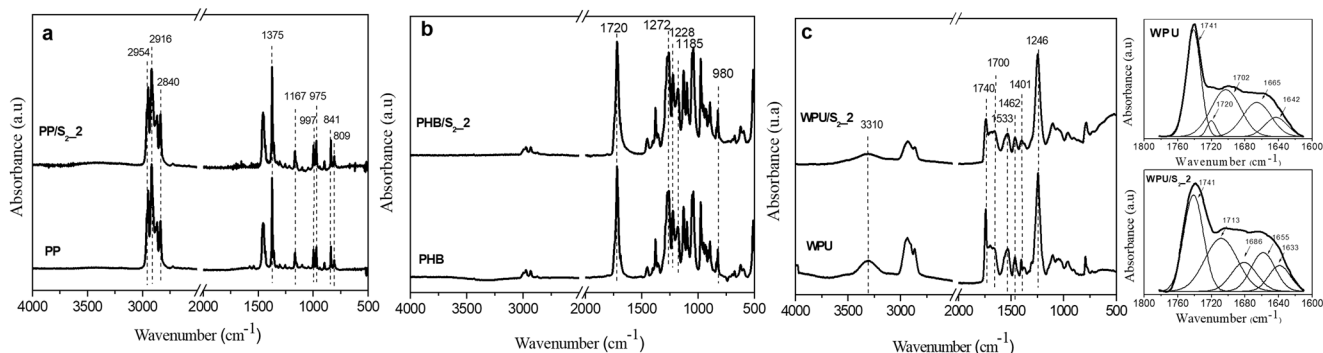


Fig. 3 FTIR spectra of pure polymer and nanocomposites (a) PP and PP/NbO₂(OH) (b) PHB and PHB/NbO₂(OH) (c) WPU and WPU/NbO₂(OH). The carbonyl band of WPU is shown on the right including the deconvolution and Gaussians adjustments (S₂ = (NbO₂(OH))

be necessary an investigation about other spectrum regions. An increase to rate R has already observed to WPU based composite and inorganic fillers [30].

The melting event T_m and crystallinity index X_c to semicrystalline polymers and nanocomposites were investigated by differential scanning calorimetry (DSC). Figure 4 shows the DSC curves to PHB and PP based materials and T_m and X_c are described in the Table 1.

In the DSC curves for WPU and WPU/NbO₂(OH) shown in Fig. 4, it was not possible to identify the melt temperature of both materials and thus, it can be suggested that there was no formation of crystals in the structure, although it is a segmented polyurethane. In the PP e PP/NbO₂(OH) curves can be observed a melting peak associated to the monoclinic crystalline phase of PP (a-PP) [31]. The T_m value of pure PP is 162 °C and to PP/NbO₂(OH) nanocomposite is 164 °C. According to Panaitescu et al. [32] in the study about SWNT in the PP matrix, a slight increase in the melting temperature may indicate small modifications interlamellar distances [32]. This behavior is accompanied by a reduction of the crystallinity index (X_c) from 44 to 33.

It can be seen a double melting peak displayed in PHB and PHB/NbO₂(OH) DSC curves (Fig. 3). However, the profile curves present differences. In contrast with PBH curve, the peak observed at lower temperature in the PHB/NbO₂(OH) curve is smaller than those in higher temperature. Double peaks are attributed to: (i) the melting, recrystallization and re-melting during the DSC scanning condition; (ii) the crystals of different families lead to different sizes of the chain polymer; (iii) the presence of two or more types of crystal (polymorphism) or (iv) structural changes in the conformation of the crystals [33, 34].

In general, a temperature shift occurred because imperfect or smaller and/or less thick crystals. The recrystallization during the melting process contributes less significantly, since the

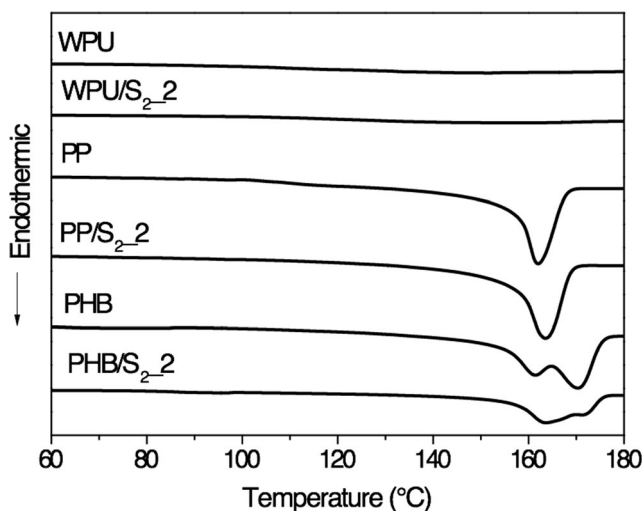


Fig. 4 DSC curve of PP e PHB polymer and PP/NbO₂(OH) e PHB/NbO₂(OH) nanocomposites ($S_2 = \text{NbO}_2(\text{OH})$)

Table 1 Thermal properties from DSC curves of semicrystalline materials ($S_2 = \text{NbO}_2(\text{OH})$)

Samples	T_m (°C)	ΔH_m (J/g)	X_{cDSC} (%)
PP	162	91	44
PP/ S_2	164	68	33
PHB	158 (T_{m1}) 169 (T_{m2})	117	80
PHB/ S_2	163 (T_{m1}) 171 (T_{m2})	103	72

double peak has already been observed in the first run. However, an exothermic event at 70 °C appears in the DSC curve indicating that the chains yet not crystallized in the cooling acquire mobility and are organized under those existing crystals.

Even as occurred to the nanocomposite PP/NbO₂(OH), the addition of NbO₂(OH) in the PHB matrix lead to a decrease of crystalline index from 80 to 72%. This result can be explained by the formation of imperfect crystals of polymers because of the reduction of the polymer chain mobility during the growth step in the presence of the nanoparticles [35]. On the other hand, the inorganic nanoparticles can act as nucleating agent promoting a disorderly growth of crystals in the interphase nanoparticle-matrix and leading to a decrease of crystals [36].

In the Fig. 5 is shown the pure polymers and nanocomposite SAXS profile. For all samples, an isotropic pattern was observed to SAXS 2D. This pattern is dependent of shape, size and size distribution of structures [37].

Figure 6 shows the scattering intensity $I(q)$ as a function of the scattering vector q and the Lorentz correction for the PP, WPU and PHB polymers and the nanocomposites containing niobium nanoparticles.

In the WPU curve can be observed of a single reflection peak related to the different micro-phases of the matrix that occurred when there was a modification of electronic density phases (Fig. 6a) [38]. The WPU used are segmented polymers presenting soft (SS) and hard segment (HS) which define the micro-phases [39, 40]. For this material, generally it can be seen the separation of these microphases during the synthesis. In addition, the properties of these materials depend on the morphology of the phase and degree of separation of the rigid and soft domains [38]. The scattering peak observed in the WPU and WPU/NbO₂(OH) occurs due to heterogeneity in the electronic density of the materials and is generally interpreted because of the presence of microphases with different electronic densities. The Lorentz correction of the WPU confirms that the material exhibits multifaceted structures, including amorphous matrix and rigid domain, as illustrated at the diagram of Fig. 7a. For WPU/NbO₂(OH) material exhibits amorphous matrix, rigid domain and nanoparticle, Fig. 7b. No peaks were observed regarding the presence of crystals in the polymeric materials, corroborating with the results in the

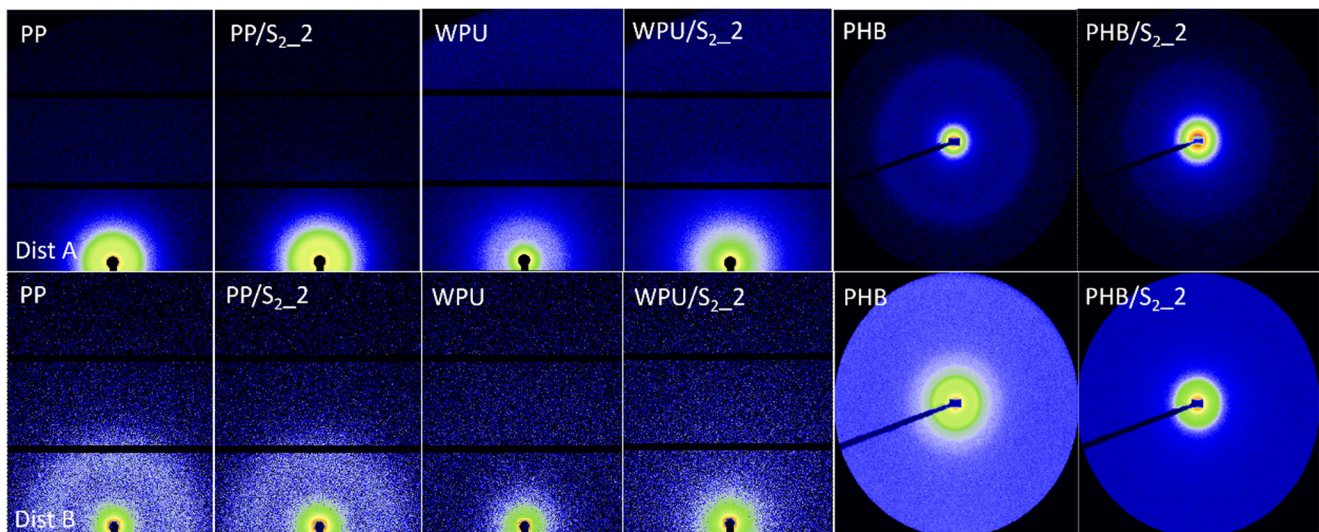


Fig. 5 SAXS pattern of polymers PP, WPU, PHB and nanocomposites polymer/NbO₂(OH) (S₂ = NbO₂(OH))

DSC. Therefore, the peak q_1 observed in the SAXS curve for the WPU and WPU/NbO₂(OH) samples refers to the rigid domains. In addition, a slope is observed in the curves of both samples in the region greater than $q = 3 \text{ nm}^{-1}$, that was associated to the WAXS region, representing structures with sub-nanometric size. This region has not investigated in this work. For the nanocomposite WPU/NbO₂(OH), it can be observed that the peak in the SAXS curve is wider and shifted to larger q values in comparison to the WPU curve. Larger peaks indicate mixtures of microphases and variation of electronic density [19].

The results obtained for the PP polymer and PP/NbO₂(OH) nanocomposite are shown in Fig. 6b. It is observed the presence of two main diffraction peaks for the pure PP curves and the PP/NbO₂(OH) nanocomposite, around $q_1 = 0,4 \text{ nm}^{-1}$ and $q_2 = 0,8 \text{ nm}^{-1}$. The ratio of the position of the peaks in the q scale shows typical values of $q; 2q$ that reveals a well-defined lamellar structure corresponding to the alternation of crystalline and amorphous regions, as can be as seen at the diagram of Fig. 7c [41]. The PP/NbO₂(OH), compared to PP, presented a slight shift of the peaks to lower values of q . This phenomenon must be attributes to the increase of lamellar periodicity resulted from

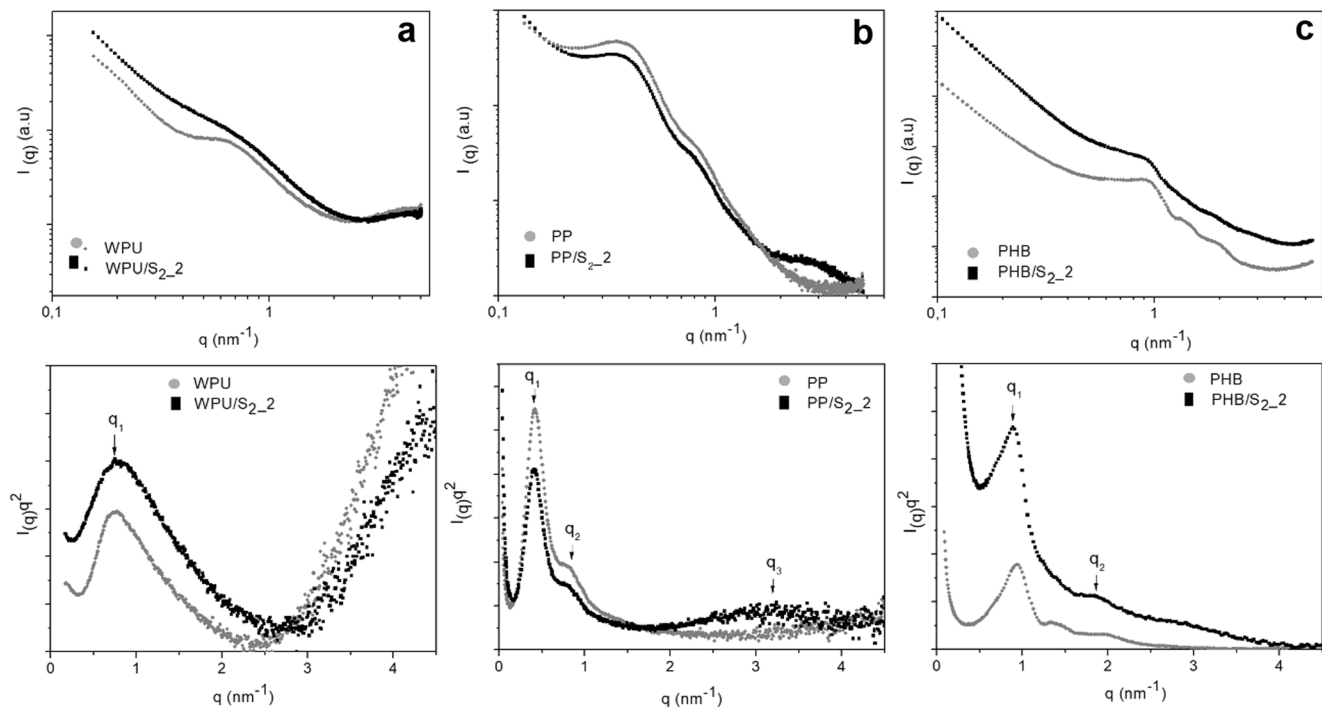


Fig. 6 SAXS curve and Lorentz correction plot of: (a) WPU, (b) PP, (c) PHB and nanocomposites polymer/NbO₂(OH) (S₂ = NbO₂(OH))

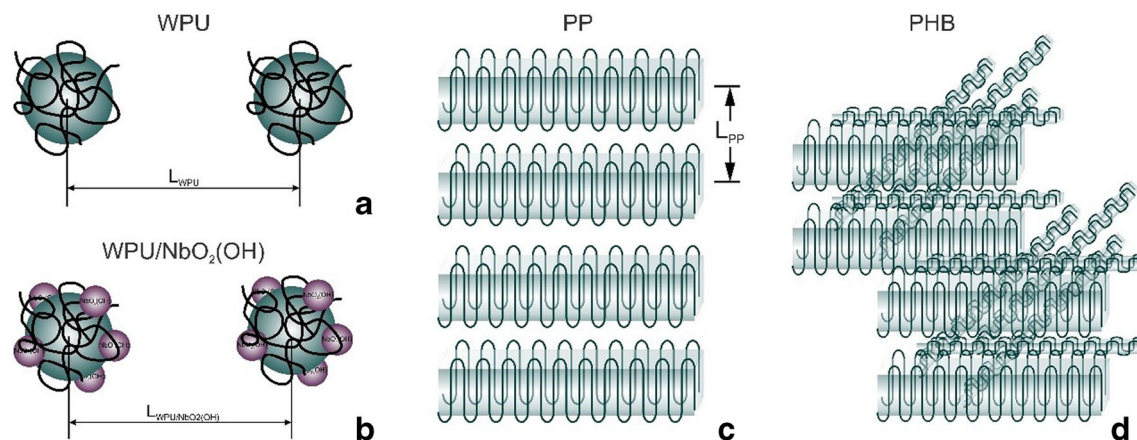


Fig. 7 Illustrated models of the polymer structures of (a) WPU, (b) PP and (c) PHB based on the results of SAXS

the introduction of the $\text{NbO}_2(\text{OH})$ particles, which indicates that the “quality” of the crystal improves, not necessarily the degree of the crystallinity increases. From DSC results, we can conclude that the nanoparticle disturbs the crystallization process and, consequently, fewer crystals are formed, but these are more perfect crystals. Furthermore, in the PP/ $\text{NbO}_2(\text{OH})$ curve we can note the presence of broad peak at $q_3 = 3.2 \text{ nm}^{-1}$ that is not observed in the PP (highlighted in Fig. 6b). This result may be related to the presence of agglomerated niobium nanoparticles in the PP matrix, as observed by Souza et al. [42]. The authors investigated the structures of modified niobium oxyhydroxide nanoparticles incorporation in PP using SAXS. In addition, the high order reflection q_3 might be represent the averaged segregation distance between the agglomerated $\text{NbO}_2(\text{OH})$ particles.

The intensity ($I(q)$) as a function of the scattering vector of the PHB and PHB/ $\text{NbO}_2(\text{OH})$ samples derived from the integration of the SAXS standards are shown in Fig. 6c. An intense peak at $q = 0.94 \text{ nm}^{-1}$ is observed in the PHB curve and secondary peaks are observed in the q range of $1.3\text{--}2.0 \text{ nm}^{-1}$. Generally, the most intense dispersion peak of semi-crystalline PHB is associated with electron density contrast alternating between crystalline and amorphous layers [43]. When the periodicity $q_1, 2q_1$ is observed, a lamellar crystalline structure is attributed to the polymer. For the materials PHB and PHB/ $\text{NbO}_2(\text{OH})$, no periodicity can be observed for the peaks. However, it suggests that part of the PHB chains did not have enough time to organize into crystalline lamellae forming different families of crystals, as shown in the DSC. In addition, the secondary peaks may be associated with formation of secondary lamellae of less thickness than the thickness of the lamellae developed during the primary phase of crystallization [44, 45] as represented at the diagram of Fig. 7d. Due to the addition of niobium nanoparticles in the PHB matrix, the higher peak, q_1 , was shifted to lower values of q and the secondary crystallization peaks were not observed. For this material, it can be observed a smaller amount of peaks, indicating the reduction of the amount of different families of crystals. The results suggest that niobium

nanoparticles led to a decrease in the formation of secondary lamellae. Moreover, the bump in the region $q = 3.02 \text{ nm}^{-1}$ is observed only for the PHB/ $\text{NbO}_2(\text{OH})$ composite is associated with the contribution of the niobium oxyhydroxide particles as discussed by Souza et al. [42]. The higher crystallinity of PHB samples was attributed to the formation of secondary and interconnected lamellae. As the nanoparticle restricted these phenomena, the X_c PHB/ $\text{NbO}_2(\text{OH})$ values are smaller.

Additionally, the morphology of the polymer was investigated by the repeating distance between the L domains. The L value is estimated from the peak position using Bragg’s Law (eq. 2) in which the peak q_1 is determined from $I(q)q^2$ versus q [46]. The values obtained for L refer to the highest intensity and well defined dispersion peak q_1 .

$$L = \frac{2\pi}{q_{max}} \quad (2)$$

The spacing L should be interpreted as the average separation distance between the domains. At WPU systems, it represents the average distance between the rigid domains. For the crystalline systems, L represents the average lamellar crystalline repeat distance.

The presence of the niobium oxyhydroxide in the WPU nanocomposite reduces the L-spacing of the pure polymer from $L_{\text{WPU}} = 8.5 \text{ nm}$ (WPU) to $L_{\text{WPU}/\text{NbO}_2(\text{OH})} = 7.8 \text{ nm}$ (WPU/ $\text{NbO}_2(\text{OH})$). Nanoparticles promote a significant difference in L-spacing and may indicate the existence of nanoparticles in the inter-domain’s regions [47]. The decrease in L spacing can also indicate the interruption of the aggregation of the chains in the rigid segment leading to the change in these regions [48]. Urethanes from the isocyanate groups can chemically interact with the hydroxyl groups of the niobium oxyhydroxide, as shown in the FTIR, by modifying the structure of the polymer chain [42]. Thus, it is proposed that the rigid domain will be more disorganized and less cohesive reducing the distance value between the rigid domains.

On the other hand, the incorporation of nanoparticles of niobium promoted a change in the L spacing between the lamellae of the polymer whose value increased slightly from $L_{PP} = 15.1$ nm to $L_{PP/NbO_2(OH)} = 5.4$ nm for the samples PP and PP/NbO₂(OH), respectively. Similar behavior was observed in the incorporation of cellulose nanoparticles in PP [49].

Conclusion

Catalytic systems based on niobium oxyhydroxide nanoparticles dispersed in different polymer matrices were obtained and applied in the removal of methylene blue by photocatalysis. The PHB/NbO₂(OH) has presented the best results achieving 90% of methylene blue removal within 60 min. Besides the excellent photocatalytic efficiency, another advantage of using the PHB/NbO₂(OH) system is the facility of the removal of the catalyst from aqueous medium since the particles are dispersed in the polymer.

The photocatalytic process involved polymer/niobium oxyhydroxide systems is dependent, mainly, of inorganic phase, influenced by size and dispersion of particles. In general, the matrix hydrophilic, WPU, led to the high dispersion of niobium oxyhydroxide which has favored the adsorption process. Although the good dispersion was achieved to the hydrophobic matrix, PP, the dye removal can be attributed to the photolysis process, mainly. In case of the system, PHB/NbO₂(OH) the photocatalytic process showed to be dependent of inorganic catalyst and of polymeric matrix. Then, interactions nanoparticles-polymer able to modify polymer properties, as crystallinity, influencing indirectly in the photocatalysis process. PHB matrix particularity, as the formation of hydroxyl radicals in the presence of UV-radiation, humidity and oxygen, improves the dye removal by photocatalysis process.

References

- López MC, Fernández MI, Martínez C, Santaballa JA (2013) Photochemistry for pollution abatement. *Pure Appl Chem* 85: 1437–1449. <https://doi.org/10.1351/PAC-CON-13-01-10>
- Chagas P, Oliveira HS, Mambri R, le Hyaric M, de Almeida MV, Oliveira LCA (2013) A novel hydrophobic niobium oxyhydroxide as catalyst: selective cyclohexene oxidation to epoxide. *Appl Catal A Gen* 454:88–92
- Pelaez M, Nolan NT, Pillai SC, Seery MK, Falaras P, Kontos AG, Dunlop PSM, Hamilton JWJ, Byrne JA, O'Shea K, Entezari MH, Dionysiou DD (2012) A review on the visible light active titanium dioxide photocatalysts for environmental applications. *Appl Catal B Environ* 125: 331–349. <https://doi.org/10.1016/j.apcatb.2012.05.036>
- Yan J, Wu G, Guan N, Li L (2014) Nb₂O₅/TiO₂ heterojunctions: synthesis strategy and photocatalytic activity. *Appl Catal B Environ* 152–153:280–288. <https://doi.org/10.1016/j.apcatb.2014.01.049>
- Byrne C, Subramanian G, Pillai SC (2017) Recent advances in photocatalysis for environmental applications. *J Environ Chem Eng* 0–1. <https://doi.org/10.1016/j.jece.2017.07.080>, 6, 3531
- Rezende CC, Neto JL, Silva AC, Lima VM, Pereira MC, Oliveira LCA (2012) Synthesis and characterization of iron/niobium composites: catalyst for dye wastewater treatments. *Catal Commun* 26:209–213. <https://doi.org/10.1016/j.catcom.2012.06.006>
- LC a O, Ramalho TC, Gonçalves M et al (2007) Pure niobia as catalyst for the oxidation of organic contaminants: mechanism study via ESI-MS and theoretical calculations. *Chem Phys Lett* 446:133–137. <https://doi.org/10.1016/j.cplett.2007.08.037>
- Rooke JC, Barakat T, Brunet J, Li Y, Finol MF, Lamonier JF, Giraudon JM, Cousin R, Siffert S, Su BL (2015) Hierarchically nanostructured porous group Vb metal oxides from alkoxide precursors and their role in the catalytic remediation of VOCs. *Appl Catal B Environ* 162:300–309. <https://doi.org/10.1016/j.apcatb.2014.06.056>
- Singh S, Mahalingam H, Singh PK (2013) Polymer-supported titanium dioxide photocatalysts for environmental remediation: a review. *Appl Catal A Gen* 462–463:178–195. <https://doi.org/10.1016/j.apcata.2013.04.039>
- Singh S, Singh PK, Mahalingam H (2015) A novel and effective strewn polymer-supported titanium dioxide photocatalyst for environmental remediation. *J Mater Environ Sci* 6:349–358
- Kasanen J, Salstela J, Suvanto M, Pakkanen TT (2011) Photocatalytic degradation of methylene blue in water solution by multilayer TiO₂ coating on HDPE. *Appl Surf Sci* 258:1738–1743. <https://doi.org/10.1016/j.apsusc.2011.10.028>
- Fostier AH, Pereira MDSS, Rath S, Guimarães JR (2008) Arsenic removal from water employing heterogeneous photocatalysis with TiO₂ immobilized in PET bottles. *Chemosphere* 72:319–324. <https://doi.org/10.1016/j.chemosphere.2008.01.067>
- Wang F, Min SX (2007) TiO₂/polyaniline composites: an efficient photocatalyst for the degradation of methylene blue under natural light. *Chinese Chem Lett* 18:1273–1277. <https://doi.org/10.1016/j.ccllet.2007.08.010>
- Heitmann AP, Patrício PSO, Coura IR, Pedrosa EF, Souza PP, Mansur HS, Mansur A, Oliveira LCA (2016) Nanostructured niobium oxyhydroxide dispersed poly (3-hydroxybutyrate) (PHB) films: highly efficient photocatalysts for degradation methylene blue dye. *Appl Catal B Environ* 189:141–150. <https://doi.org/10.1016/j.apcatb.2016.02.031>
- Heitmann Rodrigues AP, Rocha IC, Mottin AC, Carlos Alves Oliveira L, de Oliveira Patrício PS (2018) Use of poly(3-hydroxybutyrate)/niobium oxyhydroxide nanocomposites in photocatalysis: effect of preparation methods. *J Appl Polym Sci* 135:5836. <https://doi.org/10.1002/app.45836>
- Cen W, Xiong T, Tang C, Yuan S, Dong F (2014) Effects of morphology and crystallinity on the photocatalytic activity of (BiO)₂CO₃ Nano / microstructures. *Ind Eng Chem Res* 53: 15002–15011
- Souza TE, Padula ID, Teodoro MMG, Chagas P, Resende JM, Souza PP, Oliveira LCA (2015) Amphiphilic property of niobium oxyhydroxide for waste glycerol conversion to produce solketal. *Catal Today* 254:83–89. <https://doi.org/10.1016/j.cattod.2014.12.027>
- LC a O, Portilho MF, Silva AC et al (2012) Modified niobia as a bifunctional catalyst for simultaneous dehydration and oxidation of glycerol. *Appl Catal B Environ* 117–118:29–35. <https://doi.org/10.1016/j.apcatb.2011.12.043>
- Patrício PS de O, Pereira IM, Da Silva NCF et al (2013) Tailoring the morphology and properties of waterborne polyurethanes by the procedure of cellulose nanocrystal incorporation. *Eur Polym J* 49: 3761–3769. <https://doi.org/10.1016/j.eurpolymj.2013.08.006>

20. Parra DF, Rosa DS, Rezende J, Ponce P, Lugão AB (2011) Biodegradation of γ irradiated poly 3-hydroxybutyrate (PHB) films blended with poly(Ethyleneglycol). *J Polym Environ* 19:918–925. <https://doi.org/10.1007/s10924-011-0353-x>
21. Han H, Bai R (2009) Buoyant photocatalyst with greatly enhanced visible-light activity prepared through a low temperature hydrothermal method. *Ind Eng Chem Res* 48:2891–2898. <https://doi.org/10.1021/ie801362a>
22. Wacharawichanant S, Siripattanasak T (2013) Mechanical and morphological properties of polypropylene / Polyoxymethylene blends. *Adv Chem Eng Sci* 2013:202–205
23. Pinto H, Silva-cunha A, Antônio G et al (2011) Montmorillonite clay-based polyurethane nanocomposite as local triamcinolone Acetonide delivery system. *J Nanomater* 2011:1–11. <https://doi.org/10.1155/2011/528628>
24. Luna IZ, Dam KC, Chowdhury AMS, Gafur MA, Khan N, Khan RA (2015) Physical and thermal characterization of alkali treated Rice husk reinforced polypropylene composites. *Adv Mater Sci Eng* 2015:1–7
25. Velásquez J, Valencia S, Rios L, Restrepo G, Marín J (2012) Characterization and photocatalytic evaluation of polypropylene and polyethylene pellets coated with P25 TiO₂ using the controlled-temperature embedding method. *Chem Eng J* 203:398–405. <https://doi.org/10.1016/j.cej.2012.07.068>
26. Mohamed El-Hadi A (2014) Investigation of the effect of nano-clay type on the non-isothermal crystallization kinetics and morphology of poly(3(R)-hydroxybutyrate) PHB/clay nanocomposites. *Polym Bull* 71:1449–1470. <https://doi.org/10.1007/s00289-014-1135-0>
27. Ayres E, Oréfice RL (2007) Nanocompósitos derivados de dispersões aquosas de poliuretano e argila: influência da argila na morfologia e propriedades mecânicas. *Polímeros* 17:339–345. <https://doi.org/10.1590/S0104-14282007000400015>
28. Baig U, Khan AA (2015) Polyurethane-based cation exchange composite membranes: preparation, characterization and its application in development of ion-selective electrode for detection of copper(II). *J Ind Eng Chem* 29:392–399. <https://doi.org/10.1016/j.jiec.2014.12.045>
29. Ayres E, Oréfice RL, Yoshida MI (2007) Phase morphology of hydrolyzable polyurethanes derived from aqueous dispersions. *Eur Polym J* 43:3510–3521. <https://doi.org/10.1016/j.eurpolymj.2007.05.014>
30. Sadeghi M, Mehdi Talakesh M, Ghalei B, Shafiei M (2013) Preparation, characterization and gas permeation properties of a polycaprolactone based polyurethane-silica nanocomposite membrane. *J Memb Sci* 427:21–29. <https://doi.org/10.1016/j.memsci.2012.07.036>
31. Mubarak Y, Martin PJ, Harkin-Jones E (2000) Effect of nucleating agents and pigments on crystallisation, morphology, and mechanical properties of polypropylene. *Plast Rubber Compos* 29:307–315. <https://doi.org/10.1179/146580100101541111>
32. Panaitescu DM, Nicolae CA, Vuluga Z, Vitelaru C, Sanporean CG, Zaharia C, Florea D, Vasiliievici G (2016) Influence of hemp fibers with modified surface on polypropylene composites. *J Ind Eng Chem* 37:137–146. <https://doi.org/10.1016/j.jiec.2016.03.018>
33. Gunaratne LMWK, Shanks RA, Amarasinghe G (2004) Thermal history effects on crystallisation and melting of poly(3-hydroxybutyrate). *Thermochim Acta* 423:127–135. <https://doi.org/10.1016/j.tca.2004.05.003>
34. Gunaratne LMWK, R a S (2005) Melting and thermal history of poly(hydroxybutyrate-co-hydroxyvalerate) using step-scan DSC. *Thermochim Acta* 430:183–190. <https://doi.org/10.1016/j.tca.2005.01.060>
35. Wang L, He A (2015) Microstructure and Thermal Properties of Polypropylene / Clay Nanocomposites with TiCl₄ / MgCl₂ / Clay Compound Catalyst. 2015:
36. Botana A, Mollo M, Eisenberg P, Torres Sanchez RM (2010) Effect of modified montmorillonite on biodegradable PHB nanocomposites. *Appl Clay Sci* 47:263–270. <https://doi.org/10.1016/j.clay.2009.11.001>
37. Pereira IM, Oréfice RL (2011) cc. In: *Macromol Symp* pp 190–198, 299–300
38. Pereira IM, Oréfice RL (2010) The morphology and phase mixing studies on poly(ester-urethane) during shape memory cycle. *J Mater Sci* 45:369–375. <https://doi.org/10.1007/s10853-009-3969-7>
39. Laity PR, Taylor JE, Wong SS, Khunkamchoo P, Norris K, Cable M, Andrews GT, Johnson AF, Cameron RE (2004) A 2-dimensional small-angle X-ray scattering study of the microphase-separated morphology exhibited by thermoplastic polyurethanes and its response to deformation. *Polymer (Guildf)* 45:5215–5232. <https://doi.org/10.1016/j.polymer.2004.05.032>
40. Pereira IM, Oréfice RL (2010) In situ evaluation of structural changes in poly(ester-urethanes) during shape-memory cycles. *Polymer (Guildf)* 51:1744–1751. <https://doi.org/10.1016/j.polymer.2010.02.037>
41. Huang J, Xu C, Wu D, Lv Q (2017) Transcrystallization of polypropylene in the presence of polyester/cellulose nanocrystal composite fibers. *Carbohydr Polym* 167:105–114. <https://doi.org/10.1016/j.carbpol.2017.03.046>
42. Souza SD, Pereira IM, Rodrigues APH, Oliveira LCA, Boaventura TP, Souza AR, Oréfice RL, Patricio PSO (2016) Nanostructured oxyhydroxide niobium (NbO₂OH) as UV radiation protector for polypropylene. *RSC Adv* 6:5040–5048. <https://doi.org/10.1039/C5RA08514D>
43. Wasantha LM, Gunaratne K, Shanks RA (2008) Miscibility, melting, and crystallization behavior of poly(hydroxybutyrate) and poly(D,L-lactic acid blends). *Polym Eng Sci*:1683–1692. <https://doi.org/10.1002/pen>
44. Tognana S, Salgueiro W, Silva L (2015) A SAXS study of PHB/DGEBA blends crystallized at different temperatures. *Procedia Mater Sci* 8:271–277. <https://doi.org/10.1016/j.mspro.2015.04.073>
45. Heo K, Yoon J, Jin KS, Jin S, Sato H, Ozaki Y, Satkowski MM, Noda I, Ree M (2008) Structural evolution in microbial polyesters. *J Phys Chem B* 112:4571–4582. <https://doi.org/10.1021/jp711136x>
46. Zhou X, Fang C, He X, Wang Y, Yang J, Yang L, Hu J, Li Y (2017) The morphology and structure of natural clays from Yangtze River and their interactions with polyurethane elastomer. *Compos Part A Appl Sci Manuf* 96:46–56. <https://doi.org/10.1016/j.compositesa.2017.02.009>
47. Li C, Goodman SL, Albrecht RM, Cooper SL (1988) Morphology of segmented polybutadiene-polyurethane elastomers. *Macromolecules* 21:2367–2375. <https://doi.org/10.1021/ma00186a012>
48. Russo P, Lavorgna M, Piscitelli F, Acierno D, di Maio L (2013) Thermoplastic polyurethane films reinforced with carbon nanotubes: the effect of processing on the structure and mechanical properties. *Eur Polym J* 49:379–388. <https://doi.org/10.1016/j.eurpolymj.2012.11.008>
49. Mottin AC, Ayres E, Oréfice RL, Câmara JJD (2016) What changes in poly(3-Hydroxybutyrate) (PHB) when processed as electrospun nanofibers or Thermo-compression molded film? *Mater Res* 19:57–66. <https://doi.org/10.1590/1980-5373-MR-2015-0280>

Publisher's note Springer Nature remains neutral with regard to jurisdictional claims in published maps and institutional affiliations.